Supplementary Information

New insights into the pre-ignition behavior of methane behind reflected shock waves

Jesus Caravaca-Vilchez [*] **, *Karl Alexander Heufer***

Chair of High Pressure Gas Dynamics, Shock Wave Laboratory, RWTH Aachen University, 52056 Aachen, Germany

**** Corresponding author: caravaca_vilchez@hgd.rwth-aachen.de***

Table of Contents

Supplementary Information

Table of Tables

Supplementary Information

Table of Figures

Supplementary Information

1 CO_2 impact on reactivity

A sensitivity analysis for IDT has been conducted to evaluate the impact of CO_2 on the chemical kinetics of the methane mixtures. The evaluation has been done at the conditions discussed in Section 4.3.2 in the manuscript, i.e., 10 bar, 1285 K, and mixture M1. In the brute force and the direct sensitivity analyses, the sensitivity coefficient (S) is calculated as:

$$S = \frac{\ln(\tau^+/\tau^-)}{\ln(2/0.5)}$$

As shown above, either the rate constant for each reaction containing CO_2 as reactant, as well as the CO_2 collision efficiency for each third-body reaction, is increased/decreased by a factor of two, and IDTs are calculated as $\tau+$ (increased) and $\tau-$ (decreased), respectively. A positive sensitivity coefficient indicates inhibition of reactivity, whereas a negative coefficient indicates a promotion in reactivity. This sensitivity coefficient has been calculated for all reactions containing CO_2 either as reactant or as a third-body molecule. The impact of most of the reactions involving CO_2 on the IDT is considered negligible (S<0.02). The only third-body reaction that is significantly sensitive is 2 CH3 (+M) <=> C2H6 (+M), with a S factor of +0.392. However, the IDT remains nearly unchanged if the third-body efficiency of CO_2 for this reaction is either doubled or reduced to 0, indicating that the CO_2 third-body collisions do not play an important role in the ignition process of methane under the investigated conditions.

2 Experimental data summary

Table S1. Experimental data discussed in the manuscript. x_{ign}: estimated ignition position

Exp. Nº	Mix.	P5 / bar	T5 / K	IDT / ms	x_{ign} / mm
4	M1	26.98	1347.51	0.4672	67.66
5	M1	28.12	1321.5	0.528	64.41
6	M1	25.96	1272.62	0.8384	77.3
7	M1	26.49	1233.06	1.1028	-
90	M1	24.85	1232.01	0.9722	87.16
3	M1	21.91	1222.06	1.1632	-
10	M1	26.35	1203.61	1.2236	-
8	M1	26.24	1201.26	1.0786	-
89	M1	24.83	1196.77	1.2042	97.01
9	M1	24.72	1168.99	1.5442	98.87
88	M1	24.15	1156.78	1.2476	102.3
19	M1	25.04	1150.67	1.89	-
15	M1	24.79	1106.79	2.103	-
14	M1	24.1	1093.16	2.15	163.8
13	M1	24.4	1088.75	1.992	-
87	M1	24.24	1085.51	2.428	-
118	M3	25.07	1231.33	1.498	4.95
105	M2	25.18	1204.28	1.432	71.15
116	M3	24.87	1197.22	2.12	42.3
115	M3	25.05	1171.45	2.427	28.78
113	H3	24.5	1223.58	1.543	4.23
122	A3	24.91	1227.97	1.325	58.51
112	H3	24.73	1194.15	1.919	16.3
123	A3	24.77	1194.92	1.837	16.1
111	H3	25.05	1171.14	2.225	24.51
124	A3	24.47	1158.14	2.312	33.91
148	M1	10.06	1287.95	1.125	9
161	M1	9.85	1275.28	1.221	36.91
162	M1	9.79	1271.86	1.179	-
157	H1	9.97	1283.57	1.1015	11.07
158	H1	9.91	1279.82	1.182	7.7
159	H1	10.07	1289.36	1.218	12.48
166	C1	10.13	1293.98	1.404	18.79
167	C1	9.96	1284.35	1.318	21.9
183	C1	9.92	1281.77	1.401	13.76

3 Uncertainty analysis

A detailed uncertainty analysis of the experimental data helps distinguish between the different ignition modes discussed in the manuscript. Uncertainties in shock tubes are caused by multiple reasons. Particularly, the IDT data is mainly influenced by the following quantities, as suggested by [2]:

- Test temperature (T_5)
- Test pressure (P_5)
- Molar fraction of every gas that constitutes the corresponding mixture (Xi's)

T_5 and P_5, in turn, are mainly affected by potential deviations in

- Initial temperature (T_1)
- Initial pressure (P_1), only affecting P_5
- Incident shock velocity (V_s)
- Heat capacity of the fuel (C_p)
- Mole fraction (X_i)

To evaluate to what extent these quantities can impact the reported IDT data, the law of propagation of uncertainty is utilized. In the case of the IDT, this expression reads:

$$u_\tau = \sqrt{\left(\frac{\partial \tau}{\partial T_5}\right)^2 u^2(T_5) + \left(\frac{\partial \tau}{\partial P_5}\right)^2 u^2(P_5) + \sum_{i=1}^{N} \left(\frac{\partial \tau}{\partial X_i}\right)^2 u^2(X_i)}$$

Whereas the uncertainty in T_5 and P_5,

$$u_{T_5} = \sqrt{\left(\frac{\partial T_5}{\partial T_1}\right)^2 u^2(T_1) + \left(\frac{\partial T_5}{\partial V_s}\right)^2 u^2(V_s) + \left(\frac{\partial T_5}{\partial C_p}\right)^2 u^2(C_p) + \sum_{i=1}^{N} \left(\frac{\partial T_5}{\partial X_i}\right)^2 u^2(X_i)}$$

$$u_{P_5} = \sqrt{\left(\frac{\partial P_5}{\partial P_1}\right)^2 u^2(P_1) + \left(\frac{\partial P_5}{\partial T_1}\right)^2 u^2(T_1) + \left(\frac{\partial P_5}{\partial V_s}\right)^2 u^2(V_s) + \left(\frac{\partial P_5}{\partial C_p}\right)^2 u^2(C_p) + \sum_{i=1}^{N} \left(\frac{\partial P_5}{\partial X_i}\right)^2 u^2(X_i)}$$

Two distinct elements must be evaluated in these expressions: u and $\frac{\partial y}{\partial x}$. The derivative terms ($\frac{\partial y}{\partial x}$) corresponding to the conditions behind the reflected shock are calculated with a finite central difference scheme and employing the Shock and Detonation Toolbox for Cantera. The IDT partial derivatives are calculated employing the NUIG1.0Mech as chemical–kinetic model, despite the large discrepancies in the low-temperature predictions. The uncertainties of the partial quantities (u) are detailed in the next

subsections:

Initial temperature (T_1)

The measuring accuracy of the employed thermocouples at the operating initial temperature (around ±0.5K) and a potential slight inhomogeneity in the heating of the tube, might lead to a deviation from the set temperature translated into an uncertainty of +.2K. More details can be found in [3], where a detailed uncertainty analysis on the same facility is discussed.

Heat capacity (C_p)

Similarly as proposed in [3,4], an uncertainty in the heat capacity of methane of 2% is assumed.

Initial pressure (P_5)

The uncertainty in the initial pressure is affected by the accuracy of the pressure sensors used. In this work, a STS 105107 sensor with an accuracy of ±1.5mbar is used [3] in experiments execution.

Molar fractions (Xi's)

Similar to the uncertainty derived for the initial pressure, the uncertainty in the molar fractions of the test gas is influenced by the accuracy of the pressure sensors employed in the mixtures preparation. Here, a STS 105112 sensor with an accuracy of ±0.25mbar is used for the fuel filling, whereas the same sensor used for the initial pressure calculations is used for the O2 and diluents filling. Assuming a fixed gas filling order of fuel, O2 and diluents, the molar fractions of every gas are calculated as follows:

$$X_{CH4} = \frac{P_{fill,CH4}}{P_{fill,Dil}}, X_{O2} = \frac{P_{fill,O2} - P_{CH4}}{P_{fill,Dil}}, X_{N2} = 1 - \frac{P_{O2}}{P_{fill,Dil}}$$

The uncertainty of the molar fractions is calculated also applying the law of propagation of errors on the previous expressions, as follows

$$u_{X_{CH4}} = \sqrt{\left(\frac{1}{P_{fill,Dil}} u_{P_{CH4}}\right)^2 + \left(-\frac{P_{fill,CH4}}{P_{fill,Dil}^2} u_{P_{N2}}\right)^2}$$

$$u_{X_{O2}} = \sqrt{\left(\frac{1}{P_{fill,Dil}} u_{P_{O2}}\right)^2 + \left(-\frac{1}{P_{fill,Dil}} u_{P_{CH4}}\right)^2 + \left(-\frac{P_{fill,O2} - P_{fill,CH4}}{P_{fill,Dil}^2} u_{P_{Dil}}\right)^2}$$

$$u_{X_{Dil}} = \sqrt{\left(-\frac{1}{P_{fill,Dil}} u_{P_{O2}}\right)^2 + \left(\frac{P_{fill,O2}}{P_{fill,Dil}^2} u_{P_{Dil}}\right)^2}$$

Incident shock velocity (V_s)

The incident shock velocities are calculated based on the time of the arrival of the incident shock at two consecutive pressure transducers and the distance between them ($\Delta z/\Delta t$). Therefore, the uncertainty in the incident shock velocity is influenced by deviations in the pressure-time recordings and

uncertainties in the transducer's positions.

The experimental pressure traces are measured with seven PCB 113B22 ICP Pressure Sensors and recorded with a MS Instruments Transient Recorder. The incident shock causes a steep pressure rise after passing the pressure transducers. This pressure rise is not instantaneous due to the finite sensor surfaces and the sensors' rise time behavior. Analyzing the length of the continuous pressure increase of the pressure traces, which are considered as uncertainties in the sensor response, an uncertainty of ±1μs is determined, which complements to the values reported in [2,5]. For the overall time uncertainty, an additional ±0.1μs must be added to the previous value due to the limited finite sampling time of the MS Instruments Transient Recorder.

Regarding the uncertainties in the transducer positions an average deviation of 0.2% of the different positions of the velocity measurement was determined, as reported in [3]. This relative value was applied to the distance between two consecutive sensors, i.e., 140 mm.

Using the law of propagation of errors, the uncertainty in the incident shock velocity reads

$$u_{X_{Vs}} = \sqrt{\left(\frac{1}{\Delta t} u_z\right)^2 + \left(-\frac{\Delta z}{\Delta t^2} u_t\right)^2}$$

Results

This leads to the uncertainties listed in Table S2, which are of the same order of those reported in [2]. As is evident from Table S2, the uncertainties at the lower temperatures are much smaller in general due to the non-Arrhenius behavior of the test mixtures (20 % at T_5 > 1300, 10% at $T_5 < 1100$). The reader is referred to Fig. 2 in the manuscript [1]. The most relevant uncertainty affecting the IDT measurements is in T_5, whose contribution to the IDT uncertainty ranges from 0.08 to 0.25 ms. In turn, the uncertainty in the incident shock velocity and the heat capacity of the mixture has the strongest impact on the overall T_5 uncertainty, ranging from 12 to 17 K and from 3 to 5 K, respectively.

Supplementary Information

Table S2. Uncertainties in the IDT measurements.

Exp. Nº	Mix.	P5 / bar	T5 / K	u_{P_5}, %	u_{T_5}, %	u_{IDT}, %
4	M1	26.98	1347.51	2.811	1.341	19.86
5	M1	28.12	1321.5	2.786	1.321	20.19
6	M1	25.96	1272.62	2.743	1.282	18.25
7	M1	26.49	1233.06	2.706	1.250	16.47
90	M1	24.85	1232.01	2.706	1.250	19.74
3	M1	21.91	1222.06	2.701	1.242	18.79
10	M1	26.35	1203.61	2.678	1.227	16.49
8	M1	26.24	1201.26	2.676	1.225	18.90
89	M1	24.83	1196.77	2.673	1.221	17.88
9	M1	24.72	1168.99	2.647	1.198	14.77
88	M1	24.15	1156.78	2.636	1.188	18.85
19	M1	25.04	1150.67	2.630	1.183	12.17
15	M1	24.79	1106.79	2.589	1.147	10.79
14	M1	24.1	1093.16	2.578	1.136	11.80
13	M1	24.4	1088.75	2.573	1.132	9.58
87	M1	24.24	1085.51	2.570	1.129	11.09
118	M3	25.07	1231.33	2.672	1.224	15.93
105	M2	25.18	1204.28	-	-	-
116	M3	24.87	1197.22	2.642	1.197	12.36
115	M3	25.05	1171.45	2.619	1.176	11.20
113	H3	24.5	1223.58	2.884	1.354	16.79
122	A3	24.91	1227.97	2.490	1.166	16.54
112	H3	24.73	1194.15	2.856	1.328	14.45
123	A3	24.77	1194.92	2.414	1.143	13.03
111	H3	25.05	1171.14	2.836	1.308	12.85
124	A3	24.47	1158.14	2.439	1.116	10.98
148	M1	10.06	1287.95	2.842	1.294	23.27
161	M1	9.85	1275.28	2.831	1.284	22.82
162	M1	9.79	1271.86	2.830	1.282	24.01
157	H1	9.97	1283.57	3.035	1.430	25.22
158	H1	9.91	1279.82	3.032	1.427	23.94
159	H1	10.07	1289.36	3.039	1.435	22.13
166	C1	10.13	1293.98	2.862	1.275	18.47
167	C1	9.96	1284.35	2.856	1.268	20.70
183	C1	9.92	1281.77	2.855	1.266	19.73

4 Shock bifurcation phenomenon

As introduced in the manuscript, the first aspect that needs to be considered to study pre-ignition propensity in shock tubes is the origin of inhomogeneities that eventually lead to pre-ignition (Aspect #1 in manuscript [1]). It is known that the main cause of temperature inhomogeneities is the shock bifurcation, arising from the interaction of the reflected shock with the boundary layer generated by the incident shock [6].

Shock bifurcation occurs if the boundary layer is not strong enough to pass through the incident shock, and this can be evaluated by calculating the stagnation pressure of the boundary layer ($P_{0,BL}$) from [7]:

$$\begin{cases} \frac{P_{0,BL}}{P_2} = \left[1 + \frac{(\gamma-1)}{2} M_{BL}^2\right]^{\gamma/(\gamma-1)} & ,if\ M_{BL} < 1 \\ \frac{P_{0,BL}}{P_2} = \left[\frac{(\gamma-1)}{2} M_{BL}^2\right]^{\gamma/(\gamma-1)} \left[\frac{2\gamma}{(\gamma+1)} M_{BL}^2 - \frac{\gamma-1}{\gamma+1}\right]^{1/(1-\gamma)} & ,if\ M_{BL} > 1 \end{cases} \quad with\ M_{BL} = \frac{2(\gamma-1)M_2^2 + 3 - \gamma}{(\gamma+1)M_2}, \tag{1}$$

where γ is the specific heat ratio of the test gas and M the Mach number. Herein, subscript 2 refers to conditions behind the incident shock wave, and subscript 5 refers to conditions behind the reflected shock wave. If $P_{0,BL}$ is less than 0.8 times the pressure behind the reflected shock (P_5), shock bifurcation is likely to occur [6]. However, shock bifurcation would not influence the experiment if it occurs after the ignition onset. To evaluate this, a shock bifurcation time scale is defined based on the time the bifurcation height equals half of the radius (D/4) of the shock tube,

$$\tau_{BIF} = \frac{D}{4u_5 h'} \tag{2}$$

where u_5 refers to the velocity of the reflected shock. Here, the growth of the bifurcation height (h') can be assumed as constant and calculated from the empirical relation of Petersen and Hanson [7]

$$h' = 0.104 M_2^{1.07} \gamma^{-2.66} \left(\frac{W}{W_{O_2}}\right)^{-0.37} \tag{3}$$

where W stands for the molecular weight. Given the shock bifurcation timescale and the ignition delay time, the bifurcation Damköhler is formulated as

$$Da_{BIF} = \frac{\tau_{BIF}}{\tau_{IGN}}. \tag{4}$$

The Damköhler number can be plotted against the stagnation and test pressure ratio ($P_{0,BL}/P_5$). In Figure S1, three regions can be recognized. First, the unstable flow and fast chemistry region, where the shock bifurcation is likely to occur, but after the ignition onset. Second, the quasi-stable flow region,

where the shock bifurcation is unlikely to occur. Third, the undesired unstable flow and slow chemistry region, where the shock bifurcation takes place before the main ignition. Adding small amounts of He and Ar to the mixture increases the specific heat ratio of the test gas, increasing the stagnation pressure of the boundary layer ($P_{0,BL}$), according to (1). Figure S1 shows that this pressure increase is enough to avoid flow separation, indicating that He and Ar do not prevent shock bifurcation at these conditions.

Figure S1. Diagram of different bifurcation regimes in a shock tube. Representative cases from Section 4 of the manuscript [1].

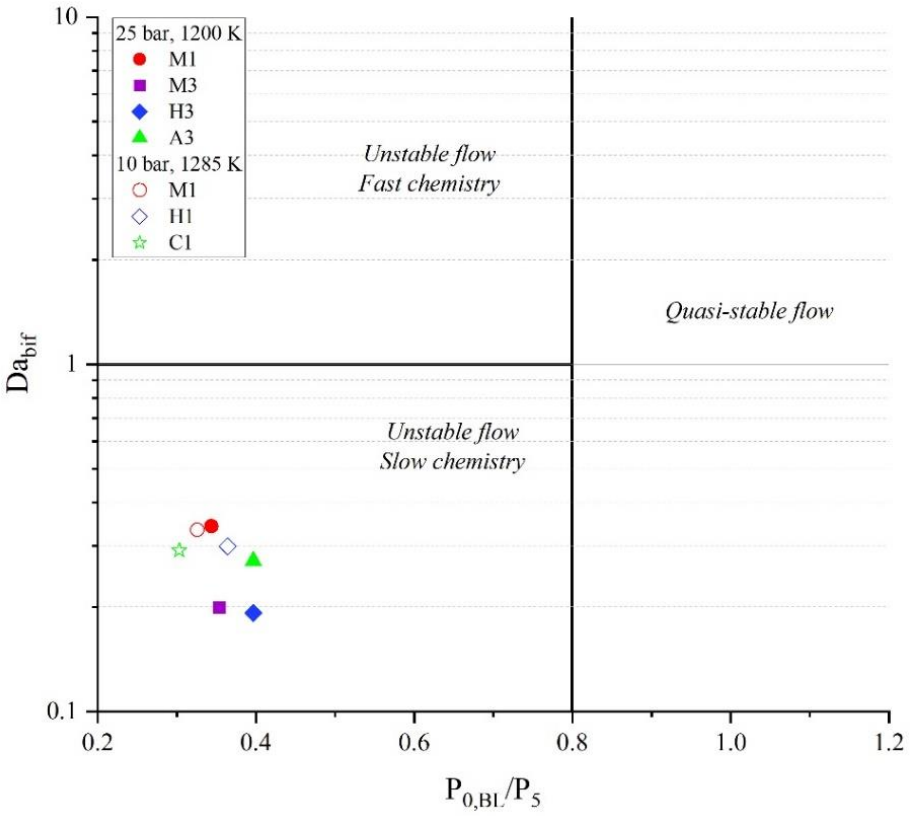

5 x-t diagram

Ignition far from the endwall is associated with pre- and mild ignitions. Independently from the ignition mode, i.e., deflagration, detonation, etc, this ignition data should not be considered in kinetic model validations. On one hand, when a localized flame kernel is formed, the test gas could be strongly affected by undesired physical effects, and therefore the assumption of the zero-dimensional transport-free auto-ignition behavior is no longer valid. On the other hand, the test conditions determined at the enwall are no longer valid if a detonation wave is formed away from the endwall. The reason is that the temperature and pressure of the bulk gas is not homogeneous, especially for those experiments undergoing strong bifurcation effects.

In this work, the x-t-diagram is proposed to identify ignition far from the endwall. The diagram is drawn based on the 7 pressure sensors that are located at the last 1 m of the shock tube. Particularly, the x-t data for four different pressure discontinuities will be determined:

Incident and reflected shock time-positions

These x-t data are directly determined from the pressure jumps corresponding to the shock wave passing over each of the 7 sensor. For every sensor, the shock time-of-arrival is taken to be the time corresponding to the maximum dP/dt. The linear shock trajectory is drawn based on the position of every sensor (red lines).

Main ignition

Similar to the previous definition, the blast wave time is determined for every sensor as the time at which the steepest pressure rise resulting from ignition is observed. Note that the blast wave (black line in Figure S2) travels at a higher velocity compared to the reflected shock wave; therefore, for some experiments, both shock wave trajectories. The blast wave is formed between the two sensors where the blast wave arrives first. Based on that assumption, two linear fits are derived from the x-t data of the sensors up- and downstream from the two selected sensors, respectively (Blast fit 1 and 2). The first fit (Blast fit 1), from the endwall sensor to the first selected sensor, defines the velocity of the blast wave. It is assumed that the blast wave travels through the x-axis at the same velocity on both sides of the ignition position, and therefore the same x-t slope is assumed between the 9 mm sensor and the other selected sensor (Blast fit 2). The intersection of the two blast fits defines the ignition position (purple star in Figure S2).

Contact surface

The contact surface defines the separation between the driven (test) gas and the driver gas. This discontinuity travels towards the endwall when the diaphragm bursts, until it interacts with the reflected shock wave at some point. At that instant, weak pressure waves might be generated which travel towards the endwall. The experiment is not longer valid if these weak waves disrupt the test gas region before ignition. The position of the contact surface is important in those experiments where the

time before ignition is longer than 2 ms [8].

Unfortunately, the passage of the contact surface is not visible on all sensors. Only a pressure minimum can be seen on the pressure trace of the first two uncoated sensors (farthest from endwall) when the contact surface passes over the sensor face. The time at which the first pressure minimum is observed, in combination with the speed of the contact surface, which is estimated by

$$u_{CS} = u_2 * (1 - \frac{\rho_1}{\rho_2})$$

enables the x-t data for the contact surface to be determined (blue line in Figure S2). According to [8], the resulting weak waves travel at the local speed of sound of the gas they occupy, i.e., the test gas. Based on that and the time-position where the reflected shock meets the contact surface, the x-t data for the resulting weak waves can be determined (dashed line in Figure S2).

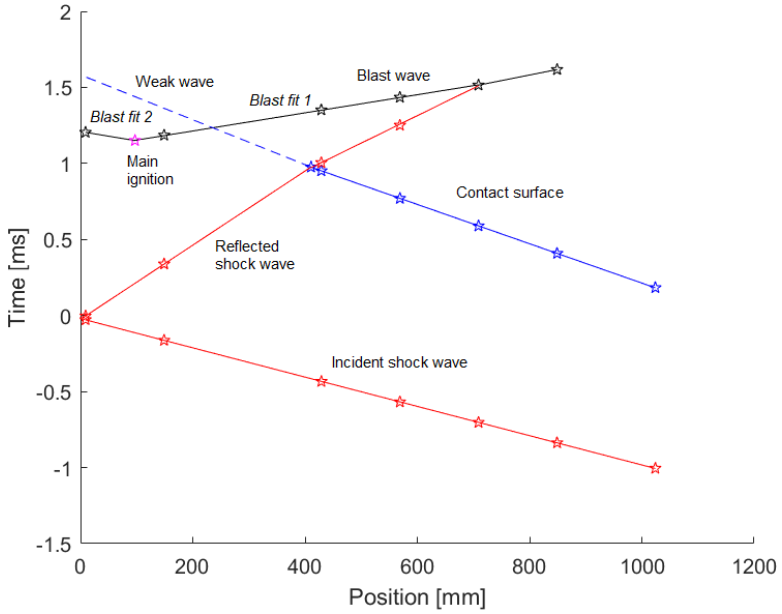

Figure S2. x-t diagram for a representative M1 experiment at 1196 K and 24.8 bar

References

1. Caravaca-Vilchez, J., Heufer, K. A., New insights into the pre-ignition behavior of methane behind reflected shock waves, Shock Waves (2022).
2. Zander, L., Vinkeloe, J., Djordjevic, N.: Ignition delay and chemical–kinetic modeling of undiluted mixtures in a high-pressure shock tube: Nonideal effects and comparative uncertainty analysis. Int. J. Chem. Kinet. 53, 611–637 (2021)
3. Minwegen, H., Burke, U., Heufer, K.A.: An experimental and theoretical comparison of C3–C5 linear ketones. Proc. Combust. Inst. 36(1), 561–568 (2017)
4. Ramalingam, K. Zhang, A. Dhongde, L. Virnich, H. Sankhla, H. Curran, A. Heufer, An RCM experimental and modeling study on CH4 and CH4/C2H6 oxidation at pressures up to 160bar, Fuel 206 (2017) 325–333
5. Baigmohammadi, M., Patel, V., Nagaraja, S.: Comprehensive experimental and simulation study of the ignition delay time characteristics of binary blended methane, ethane, and ethylene over a wide range of temperature, pressure, equivalence ratio, and dilution. Energy Fuels 34, 8808–8823 (2020)
6. Grogan, K. P., Ihme, M., Regimes describing shock boundary layer interaction and ignition in shock tubes, Proc. Combust. Inst. 36 (2) (2017) 2927–2935.
7. Petersen, E.L. , Hanson, R.K., Measurement of Reflected-shock Bifurcation Over a Wide Range of Gas Composition and Pressure, Shock Waves 15, (2006) 333–340.
8. Amadio, A.R., Crofton, M.W. & Petersen, E.L. Test-time extension behind reflected shock waves using CO2–He and C3H8–He driver mixtures. Shock Waves 16, 157–165 (2006).